Passive detection of Gaussian signals with narrow-band and broad-band components

S. Pasupathy

Department of Electrical Engineering, University of Toronto, Toronto, M5S1A4, Canada

P. M. Schultheiss

Department of Engineering and Applied Science, Yale University, New Haven, Connecticut 06520
(Received 8 June 1973)

The performance of the optimum passive detector for Gaussian signals is studied for TW (observation interval—signal spectral bandwidth) products of the order of unity. Detection and false-alarm probabilities are evaluated for carrier-symmetric bandpass signals. Conditions are then obtained under which it is preferable to use either the narrow-band or the broad-band component of the received signal. Though in most situations the results advocate processing the higher-energy component, there are situations of practical importance where the lower-energy component may be preferred.

Subject Classification: 60.30.

INTRODUCTION

The signals encountered in many passive sonar problems consist of a combination of broad-band and narrow-band components. The optimum detector clearly uses both in appropriate combination. In practice, however, one can rarely justify implementation of the optimum processor. It therefore becomes pertinent to inquire when detection should rely primarily on the narrow-band components and when the principal reliance should be placed on processing the broad-band signals. Since the narrow-band components, though often characterized by a locally high signal-to-noise ratio, frequently have a total power which is small compared to that of the broad-band components, the answer is not at all obvious.

Existing analyses of broad-band passive sonar detection have almost invariably assumed Gaussian signals and noises with a bandwidth W and observation time T satisfying $TW \gg 1$.[1-3] This assumption — generally very reasonable for the broad-band case — has two important consequences:

(1) Signal and noise can be represented by Fourier coefficients which are statistically independent. The spatial operations performed by the receiving array are then separated from the required temporal (frequency) filtering operations. The latter often become trivial and attention focuses on the spatial problem.

(2) The relatively long smoothing time T makes the detector output approximately Gaussian. Detection and false-alarm probabilities are now easily inferred from the output signal-to-noise ratio, which therefore serves as the usual figure of merit.

At the other extreme, when narrow-band signals have been analyzed, the usual assumption has been $TW \ll 1$.[4] The signal may now be regarded as a sinusoid with unknown phase and analytical treatment becomes once again possible.

The narrow-band signals of interest to us fall into neither of the above categories. We certainly can not assume $TW \gg 1$. On the other hand, we do not wish to postulate the extreme degree of frequency stability implied by $TW \ll 1$. We are therefore forced to seek different methods for avoiding the analytical difficulties sketched above.

Our approach to separating space and time operations is the opposite of case (1). While the large TW assumption trivializes the time-filtering operation and centers attention on the spatial problem, we trivialize the spatial problem (by assuming white noise independent from sensor to sensor) and focus our attention on the temporal-filtering problem. We circumvent the difficulty of dealing with a non-Gaussian system output in computing the detection and false-alarm probabilities by somewhat restricting the class of allowed narrow-band signals. This leads to probabilities in the form of series which converge rapidly for the parameter values of interest.

I. THE LIKELIHOOD RATIO DETECTOR

A block diagram of the array processor is shown in Fig. 1. The receiving array may have arbitrary geometry. Without loss of generality we may assume that the output of each sensor has been delayed sufficiently so that the various signal components are aligned. The output of the jth sensor, suitably delayed, will be designated as $r^j(t) = \alpha s^j(t) + n^j(t)$, where $s^j(t)$ and $n^j(t)$ are the signal and noise waveforms, respectively. α is unity if a signal is present and zero if it is not. With the assumed alignment of signals $s^j(t) = s(t)$, for all j. We may then represent our entire data set by the vector $\mathbf{r}(t)$, whose components are the $r^j(t)$. Each of the $r^j(t)$ is in turn represented (for the moment) by an arbitrary orthonormal expansion

$$r^j(t) = \sum_{i=1}^{\infty} r_i^j \phi_i(t) , \tag{1}$$

$$r_i^j = \int_{-T/2}^{T/2} r^j(t) \phi_i(t)\, dt . \tag{2}$$

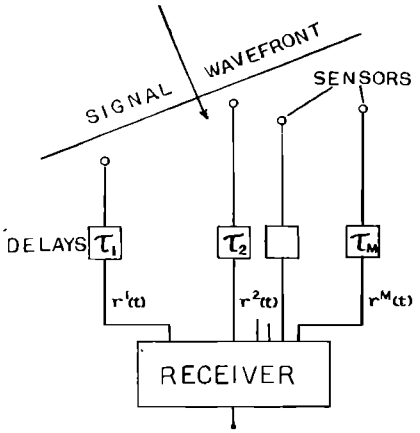

FIG. 1. A passive array processor.

We make the following assumptions:

(1) Signal and noise are independent stationary Gaussian processes. The signal has a known correlation function $R(\tau)$.

(2) The noise is white and independent from sensor to sensor. Its spectral density is the constant N.

Under these assumptions the obvious choice for the orthonormal set $\{\phi_i(t)\}$ is the set of eigenfunctions of the Karhunen–Loève equation

$$\int_{-T/2}^{T/2} R(t-u)\phi_i(u)\,du = \lambda_i \phi_i(t)\,. \tag{3}$$

Well-known computational procedures now lead to the structure of the optimum (likelihood ratio) detector. The detector output is

$$u = \sum_{i=1}^{\infty} \frac{\lambda_i}{N(M\lambda_i + N)} \left(\sum_{j=1}^{M} r_i^j \right)^2, \tag{4}$$

where M is the number of sensors. Figure 2 shows a block diagram of the detector specified by Eq. 4. Spatial processing is seen to consist of nothing more than conventional beamforming. The array has become equivalent to a single sensor with improved signal-to-noise ratio. Since Eq. 2 is a linear operation on the $r^j(t)$ and $\mathbf{r}(t)$ is Gaussian, the sums $\sum_{j=1}^{M} r_i^j$ appearing in Eq. 4 are zero-mean Gaussian random variables with variance

$$D^2\left(\sum_{j=1}^{M} r_i^j \right) = N + \alpha M \lambda_i, \quad \alpha = 0,\ 1\,. \tag{5}$$

A straightforward, though somewhat tedious, computation now yields the characteristic function of the detector output u.

$$\psi(x) = \prod_{i=1}^{\infty} (1 - 2jx\sigma_{\alpha i})^{-1/2}, \tag{6}$$

where

$$\sigma_{\alpha i} = \frac{M\lambda_i}{N + \alpha M \lambda_i}, \quad \alpha = 0,\ 1\,. \tag{7}$$

Fourier inversion of Eq. 6 leads to the probability density $p(u)$ which can, in turn be integrated to obtain the detection and false-alarm probabilities. The computational problems involved are not trivial.[6,7] The literature contains analytical results for very weak signals,[8] very small TW products,[9] and for bounds on the detection and false alarm probabilities[5] — none of which are conditions well matched to our requirements. Numerical procedures for computing the cumulative distribution function directly from the characteristic function have been described by Nuttall[10,11] and Wang.[12] Similar techniques could undoubtedly be used here. Instead we take a somewhat different approach, restricting attention to a particular signal model which leads to relatively simple analytical manipulations and postpones numerical procedures to the final step.

II. CARRIER–SYMMETRIC BANDPASS SIGNALS

The narrow-band signal process we want to model can be assumed to be a bandpass process centered about a carrier frequency ω_0. We shall further assume that the signal power spectrum is *symmetric* about the carrier.

The received waveforms are processed as shown in Fig. 3 to yield two waveforms $Z_1(t)$ and $Z_2(t)$. These, instead of the single waveform $\sum_{i=1}^{M} r^i(t)$ used in Fig. 2,

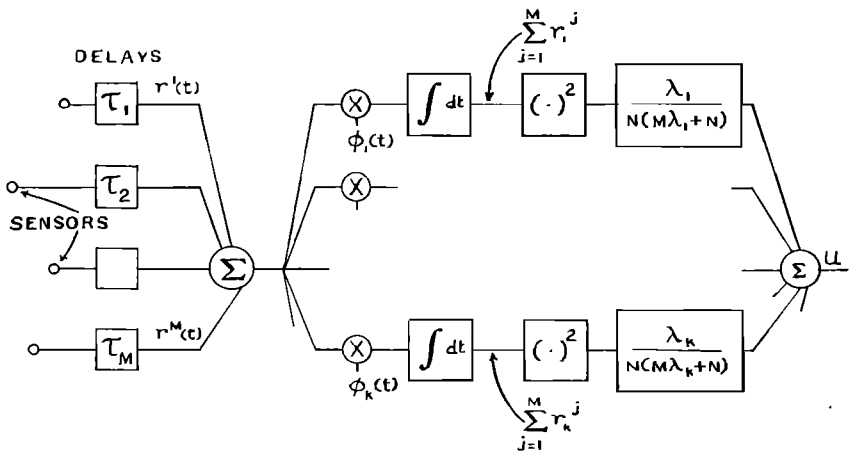

FIG. 2. Optimum detector.

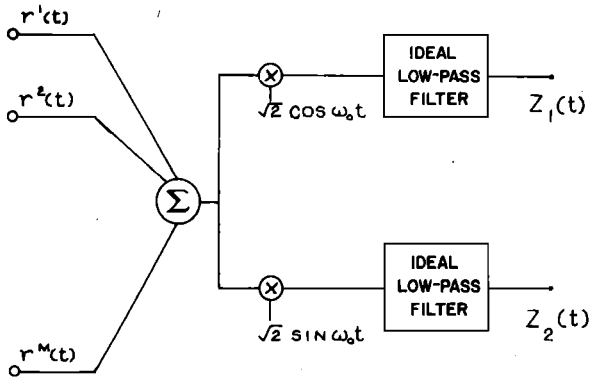

FIG. 3. Low-pass representation of bandpass signals.

form the inputs for the likelihood ratio test:

$$Z_i(t) = \alpha s_i(t) + n_i(t), \quad i = 1, \ 2 \ . \tag{8}$$

The following properties of the demodulated low-pass signals $s_1(t)$ and $s_2(t)$ follow immediately.[13]

(1) Since the input signal $s(t)$ is wide-sense stationary, $s_1(t)$ and $s_2(t)$ are also wide-sense stationary. They have the same power spectrum, which is just the low-pass component of the bandpass spectrum after it has been shifted to the origin. It follows that the eigenvalues of $s_1(t)$ and $s_2(t)$ are the same.

(2) Since the bandpass process is symmetric about the carrier, $s_1(t_1)$ and $s_2(t_2)$ are uncorrelated for all observation instants t_1 and t_2. The Gaussian assumption then makes $s_1(t)$ and $s_2(t)$ independent.

Examples of carrier symmetric bandpass signals occur often enough in radar, sonar, and communication problems[14] to make the class a practically interesting one.

III. ERROR PROBABILITIES

The two low-pass processes $Z_1(t)$ and $Z_2(t)$ can be processed separately (since they are independent) and then combined to generate the approximate statistic (see Eq. 4):

$$u = \sum_{i=1}^{k} \frac{\lambda_i}{N(M\lambda_i + N)} (Z_{1i}^2 + Z_{2i}^2) \ , \tag{9}$$

where

$$Z_{ni} = \int_{-T/2}^{T/2} Z_n(t) \, \phi_i(t) \, dt, \quad n = 1, \ 2 \ . \tag{10}$$

Equation 9 is approximate because the sum is terminated at $i = k$. Since $\sum_{i=1}^{\infty} \lambda_i = R(0)$, a finite number, there is clearly a finite k such that the cumulative contribution to Eq. 4 of all terms $i > k$ is negligible. In fact, it will become apparent shortly that the k required for the problem of interest here can be quite small.

$s_1(t)$ and $s_2(t)$ have the same spectrum; hence the characteristic functions of Z_{1i} and Z_{2i} are the same. Also, since they are independent, the characteristic function of u is (Eq. 6)

$$\psi(x) = \prod_{i=1}^{k} (1 - 2jx\sigma_{\alpha i})^{-1} \ . \tag{11}$$

The probability density function of u can now be calculated exactly:

$$p(u) = \sum_{i=1}^{k} a_{\alpha i} \exp\left(-\frac{u}{2\sigma_{\alpha i}}\right), \quad u \geq 0 \ ,$$
$$= 0 \ , \qquad u < 0 \ , \tag{12}$$

where

$$a_{\alpha i} = \left[\frac{(\sigma_{\alpha i})^{k-2}}{2}\right] \prod_{\substack{j=1 \\ j \neq i}}^{k} \frac{1}{(\sigma_{\alpha i} - \sigma_{\alpha j})} \ . \tag{13}$$

The probability of detection is

$$P_d = \int_{\gamma}^{\infty} p(u \mid \alpha = 1) \, du = \sum_{i=1}^{k} b_{1i} \exp\left(-\frac{\gamma}{2\sigma_{1i}}\right), \quad \gamma > 0 \ , \tag{14}$$

and the probability of false alarm is

$$P_f = \int_{\gamma}^{\infty} p(u \mid \alpha = 0) \, du = \sum_{i=1}^{k} b_{0i} \exp\left(-\frac{\gamma}{2\sigma_{0i}}\right), \quad \gamma > 0 \ , \tag{15}$$

where

$$b_{\alpha i} = \prod_{\substack{j=1 \\ j \neq i}}^{k} \frac{\sigma_{\alpha i}}{(\sigma_{\alpha i} - \sigma_{\alpha j})} \tag{16}$$

and γ is the detection threshold.

IV. DETECTION OF NARROW-BAND VERSUS BROAD-BAND SIGNAL COMPONENT

We now turn to the problem which motivated this study. Consider a narrow-band signal with the low-pass equivalent spectrum

$$S_L(\omega) = H \ , \quad |\omega| \leq 2\pi W \ ,$$
$$= 0 \ , \quad \text{otherwise} \ . \tag{17}$$

The eigenvalues and eigenfunctions for this well-known spectrum have been tabulated.[15] Since we are interested in small TW products and since there are only approximately $2TW$ significant eigenvalues for the above spectrum, the number of terms k in Eqs. 14 and 15 need not be too large to get accurate results. Also, from Eqs. 7 and 16, we see that both $\sigma_{\alpha i}$ and $|b_{\alpha i}|$ decrease rapidly for higher-order eigenvalues. All of these factors ensure rapid convergence of the expressions for P_d and P_f.

Let us introduce several new symbols to emphasize the important parameters in the performance characteristics. Let

$$C = \pi WT \ , \tag{18}$$

which is a measure of the time–bandwidth product of the signal

$$E = CMH$$
$$= (\pi HWT) M \ , \tag{19}$$

which, for constant M, is a measure of the average signal energy

$$A = HM/N, \tag{20}$$

which, for constant M, is a measure of the signal-to-noise ratio in the signal band. Notice that $CA = E/N$.

In Fig. 4 we plot the probability of detection as a function of C, the normalized TW product. The false-alarm probability is fixed at 10^{-5} in Fig. 4(a) and at 10^{-3} in Fig. 4(b). The solid curves in each instance describe system performance for a given normalized signal energy E/N, while the dashed curves specify system performance for a given signal-to-noise ratio A in the signal band.

Perhaps the single most important feature of Figs. 4(a) and 4(b) is the qualitative difference between the fixed-energy curves near the top and those near the bottom of the graphs. The high-energy curves near the top of the diagrams have a small but definitely positive slope. (Note that P_d has been plotted logarithmically.) The low-signal-energy curves exhibit a negative slope which becomes more pronounced as the signal energy decreases. Thus, there is a threshold value V_t above which an increase of bandwidth leads to improved detection performance. Below the threshold there is a definite premium on the use of narrow bandwidth.

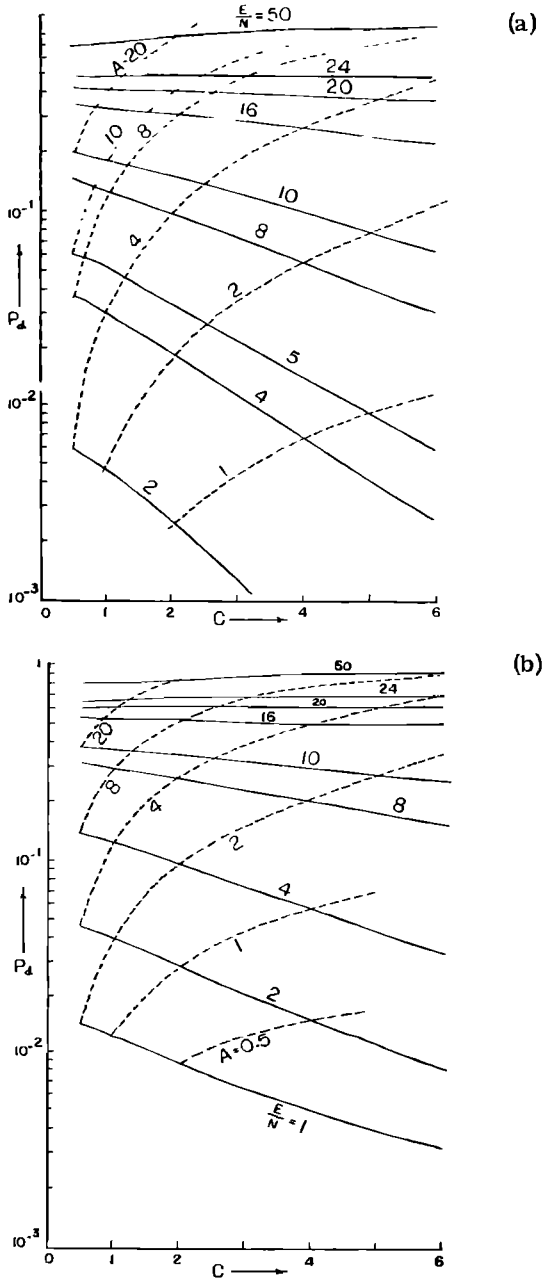

FIG. 4. Detection probability P_d vs normalized time–bandwidth product C. —— constant (E/N). – – – constant A. (a) $P_f = 10^{-5}$; (b) $P_f = 10^{-3}$.

Now consider the following practical problem. A received signal is known to contain a broad-band component and a narrow-band component. We want to find a simple criterion that will enable us to determine which of the two makes the dominant contribution to the detection process. (Extensions to several narrow-band components are straightforward.) There are six possible combinations of the relative magnitude of wide-band E/N, narrow-band E/N, and threshold value:

(1) $(E/N)\text{w.b.} \geq (E/N)\text{n.b.} > V_t$,

(2) $(E/N)\text{n.b.} > V_t > (E/N)\text{w.b.}$,

(3) $(E/N)\text{w.b.} > V_t > (E/N)\text{n.b.}$,

(4) $V_t > (E/N)\text{n.b.} \geq (E/N)\text{w.b.}$,

(5) $(E/N)\text{n.b.} > (E/N)\text{w.b.} > V_t$,

(6) $V_t > (E/N)\text{w.b.} > (E/N)\text{n.b.}$.

In cases (1)–(4) qualitative inspection of the performance curves is sufficient to make the choice: in each case the *higher-energy* component is clearly preferable. In cases (5) and (6) one must look more carefully. In case (5) the narrow-band signal lies near the left end of the higher-energy curve. The broad-band signal lies on the right side of its (rising) curve and may therefore be preferable in spite of its lower total energy. The opposite situation can occur in case (6). Both E/N values are below threshold, and now the negative slope of the performance curves can easily be sufficient to offset the basic energy advantage of the wide-band signal.

The general conclusion therefore is: one always prefers the component with higher energy *unless* (1) both E/N values are above threshold and the narrow-band component is stronger, or (2) both E/N values are below threshold and the wide-band component is stronger. In these two cases a more careful examination of the performance curves is indicated.

Figure 5 represents an attempt to indicate the dependence of V_t on the false-alarm probability. The definition of V_t has an element of arbitrariness because there is no single value of E/N for which the performance curve is entirely horizontal. However, it is clear from Fig. 5 that the transition from predominantly positive slope to predominantly negative slope occurs at lower and lower energy levels as the allowed false-alarm probability increases.

If one attempts to look at the same problem from the point of view of signal-to-noise ratio A rather than nor-

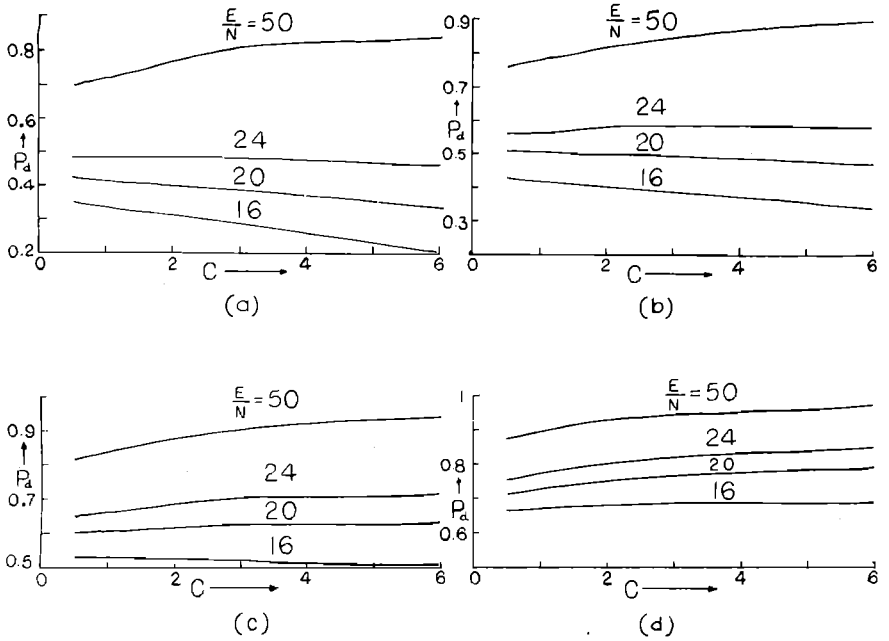

FIG. 5. Relation between threshold energy and false-alarm probability P_f. (a) $P_f = 10^{-5}$; (b) $P_f = 10^{-4}$; (c) $P_f = 10^{-3}$; (d) $P_f = 10^{-2}$.

malized signal energy E/N, the results are much less informative. All of the constant A (dashed) curves in Fig. 4 rise sharply from left to right. When the signal-to-noise ratio (in the signal band) of the wide-band component exceeds that of the narrow-band component, the wide-band component is clearly preferable. This is a correct but trivial conclusion. However, short of a detailed study of numerical values, it is not at all evident how much larger the signal-to-noise ratio of the narrow-band component must be before it begins to dominate the detection process. Discrimination on the basis of relative energy appears to be by far the more useful approach.

V. CONCLUSIONS

The performance of the optimum array detector was studied for TW products of the order of unity. Carrier symmetric bandpass signals were used to simplify the analysis. Conditions were obtained under which it is preferable to use either the narrow-band component or the broad-band component of the received signal. Though in most situations the results advocate processing the higher-energy component, there are clear situations of practical importance when a lower-energy component would be preferred.

It should also be mentioned that by focusing attention on the spatial part of the optimum processor, one can pose the parallel problem of determining the detector performance for small BL (spatial bandwidth length of array) products. The analysis and results of this study remain applicable with trivial modifications.

ACKNOWLEDGMENT

The research reported in this paper was supported in part by the Naval Underwater Systems Center, New London, Connecticut, under Contract N00140-72-C-1293.

[1]F. Bryn, "Optimal Signal Processing of Three-Dimensional Arrays Operating on Gaussian Signals and Noise," J. Acoust. Soc. Am. 34, 289–297 (1962).
[2]W. Vanderkulk, "Optimum Processing for Acoustic Arrays," J. Brit. IRE 26, 285–292 (1963).
[3]D. J. Edelblute, J. M. Fisk, and G. L. Kinnison, "Criteria for Optimum Signal Detection Theory for Arrays," J. Acoust. Soc. Am. 41, 199–205 (1967).
[4]H. L. Van Trees, *Detection, Estimation and Modulation Theory* (Wiley, New York, 1968), Pt. I, Chap. 4.
[5]Ref. 4, Pt. III, Chaps. 2 and 3.
[6]D. Slepian, "Fluctuations of Random Noise Power," B.S.T.J. 37, 163–184 (1958).
[7]Ref. 5, p. 33.
[8]I. Selin, *Detection Theory* (Princeton U.P., Princeton, N.J., 1965).
[9]J. I. Marcum, "A Statistical Theory of Target Detection by Pulse Radar," IEEE Trans. Inform. Theory 6, 59–267 (1960).
[10]A. H. Nuttall, "Numerical Evaluation of Cumulative Probability Distribution Function Directly from the Characteristic Function," Proc. IEEE 57, 2071–2072 (Nov. 1969).
[11]A. H. Nuttall, "Alternative Forms and Computational Considerations of Numerical Evaluation of Cumulative Probability Distributions Directly from Characteristic Functions," NUSC Rep. No. NL-3012 (Aug. 1970).
[12]L. Wang, "Numerical Calculation of Cumulative Probability from the Moment-Generating Function," Proc. IEEE 60, 1452–1453 (Nov. 1972).
[13]Ref. 5, Appendix A.3.1.
[14]Ref. 5, Chap. 11.
[15]C. Flammer, *Spheroidal Wave Functions* (Stanford U.P., Stanford, Calif., 1957).